Imaging of Polar Mesosphere Summer Echoes with the 450 MHz Poker Flat Advanced Modular Incoherent Scatter Radar

M. J. Nicolls,[1] C. J. Heinselman,[1] E. A. Hope,[1] S. Ranjan,[1] M. C. Kelley,[2] and J. D. Kelly[1]

Received 2 August 2007; revised 24 August 2007; accepted 5 September 2007; published 16 October 2007.

[1] Polar Mesosphere Summer Echoes (PMSE) occur near the mesopause during the polar summer months. PMSE are primarily studied at VHF, however there have been some detections at higher frequencies. Here, we report on some of the first detections of PMSE with the 450 MHz (67 cm) Poker Flat Advanced Modular Incoherent Scatter Radar (PFISR). Echoes were observed with volume reflectivities (radar scattering cross section per unit volume) near $2–3 \times 10^{-17}$ m^{-1}. On 11 June 2007, PFISR was operating in a 26-beam position mode, with look directions spread over an approximately 80 by 80 km^2 region at 85 km altitude with elevation angles as low as $\sim$50°. The measurements showed patchy (tens of kilometer) irregularity regions drifting in from the north, in addition to smaller, more localized structures. There was no evidence for strong aspect sensitivity of these UHF echoes, as PMSE was observed in all look directions with relatively uniform intensity. The observations indicate the presence of fossilized irregularities drifting with the background wind field as well as areas of developing irregularities possibly associated with the presence of active neutral air turbulence.
Citation: Nicolls, M. J., C. J. Heinselman, E. A. Hope, S. Ranjan, M. C. Kelley, and J. D. Kelly (2007), Imaging of Polar Mesosphere Summer Echoes with the 450 MHz Poker Flat Advanced Modular Incoherent Scatter Radar, *Geophys. Res. Lett.*, *34*, L20102, doi:10.1029/2007GL031476.

1. Introduction

[2] The polar summer mesosphere region is the coldest place on Earth, with minimum temperatures close to 130 K. Even with very low water vapor levels, this frigid environment can lead to the formation of ice crystals and noctilucent clouds (NLC), which have been observed and studied for over a century. Polar mesosphere summer echoes (PMSE) are the coherently scattered returns from irregularities occurring at the Bragg scattering wavelength that form in the polar mesopause region. PMSE were first discovered in the late 1970s when they were shown to exhibit a strong seasonal variation at VHF [*Czechowsky et al.*, 1979; *Ecklund and Balsley*, 1981; *Balsley et al.*, 1983]. For a summary of the current understanding of PMSE, we refer the reader to the most recent review articles [*Cho and Röttger*, 1997; *Rapp and Lübken*, 2004].

[3] The prevailing explanation for PMSE is as follows. The ice particles that develop in the polar mesopause become charged, and the multi-component plasma subsequently exhibits a reduced diffusion coefficient. The turbulent velocity field resulting from gravity wave breaking leads to small-scale structuring in the neutral fluid with outer scales of tens of meters. Some extension of the turbulent energy cascade is necessary to explain observations of PMSE at VHF and beyond.

[4] It has been shown [*Kelley et al.*, 1987; *Kelley and Ulwick*, 1988] that charged ice particles extend the electron density irregularity spectrum. This theory, however, requires the presence of active neutral air turbulence during times of PMSE, a prediction not always fulfilled by observation [*Lübken et al.*, 1993, 2002]. *Rapp and Lübken* [2003] later demonstrated that the plasma structures acquire a long lifetime because of reduced electron diffusivity, decoupling the existence of small-scale structures from active turbulence. Measurements of aspect sensitivity and an inverse relationship between scattering cross-section and spectral width suggest that scattering from steep (non-turbulent) edges may also play a role [*Röttger et al.*, 1990; *Alcala and Kelley*, 2001]. Steep edges also require a low plasma diffusion coefficient. However, recently *Rapp and Hoppe* [2006] postulated that the observed anti-correlation between spectral width and echo intensity may be explained by turbulent scatter based on the mixing properties of breaking gravity waves.

[5] PMSE have primarily been studied with VHF systems at probing angles close to zenith. The backscattering cross section for PMSE drops significantly with increasing frequency, over 6 orders of magnitude from 50 to 500 MHz [*Rapp and Lübken*, 2004]. There have only been a few detections of PMSE at UHF, by the EISCAT 933 MHz (32 cm) system [*Rottger et al.*, 1990; *La Hoz et al.*, 2006], the EISCAT Svalbard (ESR) 500 MHz (60 cm) system [*Hall and Rottger*, 2001], and the Sondrestrom 1.29 GHz (23 cm) system [*Cho et al.*, 1992]. A recent comprehensive study [*La Hoz et al.*, 2006] highlights the inability of any theory to adequately explain observations of PMSE at UHF. In this paper, we present observations of PMSE with the 450 MHz (67 cm) Poker Flat Incoherent Scatter Radar (PFISR), the multi-beam capability of which can be used to investigate previously irreconcilable aspects of PMSE morphology at UHF.

2. Experiment Description

[6] PFISR is located at the Poker Flat Research Range (65.13°N, 147.47°W) near Fairbanks, Alaska. PFISR has the ability to steer on a pulse-to-pulse basis, providing a

[1]Center for Geospace Studies, SRI International, Menlo Park, California, USA.
[2]School of Electrical and Computer Engineering, Cornell University, Ithaca, New York, USA.

0094-8276/07/2007GL031476$05.00

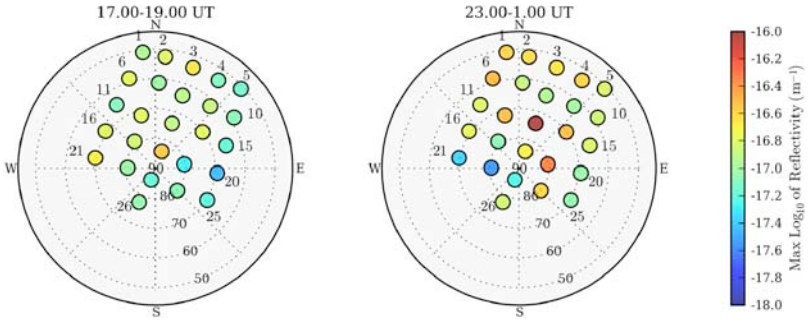

Figure 1. Log_{10} of maximum reflectivity from the 82 to 87 km altitude region for all 26 beams within the two time periods indicated for 11–12 June 2007.

powerful extension over typical ISRs. The radar is tilted so that its boresight direction corresponds to elevation and azimuth angles of 74° and 15°, respectively. The beamwidth of PFISR is about 1° × 1.5°, with the larger dimension in the plane perpendicular and north to the radar face. The experimental configuration used here employed 26 beam positions at a range of pointing angles centered around the boresight direction. The azimuths and elevations of the 26 beams are shown in Figure 1. Twenty-five beams form a 5 × 5 rectangular pattern, and the 26th beam looks up the magnetic field line, *B*. The rectangular pattern is rotated east of north, and at these altitudes (∼85 km) covers an extent of ∼62 by 68 km. Note that there is no beam pointed exactly vertically. The color coding of Figure 1 is discussed later.

[7] The experimental mode consisted of transmitting 10 μs (1.5 km), 13-baud barker coded pulses on two frequencies (449.6 and 449.3 MHz) to best use the available 10% duty cycle of the system. A long pulse was also transmitted but will not be discussed. We note that this experimental setup is not conducive for PMSE spectral studies. The data were integrated online for 16 seconds, corresponding to ∼128 pulses per direction per frequency. The total power of the 96-panel PFISR is ∼1.3 MW.

3. Observations

[8] Figure 2 summarizes the observations on 11–12 June 2007. The observations extended from ∼15 UT on the 11th until ∼03 UT on the 12th (LT is Alaska Daylight Time, UT-8 hours). The data are plotted as the $\log_{10}$ of radar scattering cross section per unit volume, commonly referred to as the volume reflectivity, as a function of time and altitude (75–100 km), for all 26 beams. The color limits cover the reflectivity range 10^{-18} to $10^{-16.8}$ m^{-1}. The reflectivity is computed as, $\eta = \frac{P_r}{P_t}\frac{\sigma_e}{\tau_p k_{sys}} r^2$ m^{-1} where P_r and P_t are the received and transmitted power, $\sigma_e \approx 10^{-28}$ m^2 is the radar scattering cross section for a single electron, τ_p is the pulse width, k_{sys} is a system constant in units of m^5 s^{-1}, and r is the range. Note that for incoherent scattering at probing angles sufficiently far from perpendicular and neglecting Debye length effects, $\eta \approx N_e\sigma_e / (1 + T_e/T_i)$ where N_e is the electron density and T_e/T_i is the electron to ion temperature ratio. k_{sys} has been determined with a careful calibration using daytime plasma line measurements. For a phased array, k_{sys} is a function of the look direction off boresight (and is also affected by other parameters, such as proximity to grating lobe limits). We estimate k_{sys}, and the derived reflectivity, to be accurate within about 10%.

[9] The plots in Figure 2 are organized so that the rows of plots (top to bottom) go from north to south and the columns go from west to east (see locations and labels indicated in Figure 1). The data in the first 26 panels have been averaged for 16 seconds and then combined with a 5-minute median to remove meteors and other sporadic returns. This accumulation corresponds to about 4800 pulses per direction, and is done mainly to reduce background fluctuations to reasonable levels so that the PMSE are easily discernible on this long-duration (>10 hour) plot. This procedure naturally filters out some of the shorter-lived echoes, but gives us confidence that the observed backscatter is statistically significant.

[10] Two main patches of echoes can be clearly seen, the first between 17–18 UT and the second from 23–01 UT, occurring at 80–90 km altitude. The two patches of echoes are observed in some form in all 26 beams, although they are stronger and longer-lived in the northern-most beams. In addition, there are shorter-lived, more sporadic patches in several of the beams that are not observed in all look directions. The altitude regime of the echoes and their temporal behavior are consistent with other UHF observations [*Röttger et al.*, 1990; *Hall and Röttger*, 2001; *La Hoz et al.*, 2006] and indicate fairly conclusively that these are indeed PMSE. June 11 is quite early in the PMSE season and these echoes are longer lasting and cover more range gates than the EISCAT Svalbard (ESR) 500 MHz results.

[11] To illustrate some of the structure of the echoes, in the three panels in the lower right of Figure 2 we zoom in on the white-boxed regions (80–90 km, ∼2315–01 UT) of beams 2, 3, and 4, corresponding to the center region of the northern-most row of beams. The data in these plots have been accumulated for 1 minute (∼1024 pulses). The zoomed-in subplots show patches of echoes centered at ∼85 km and extending ∼4 km, lasting for tens of minutes. While the echoes are observed in all three beams, there is significant spatial variation over this region (the horizontal distance between adjacent beams is ∼17 km at 85 km altitude). Beams 2 and 3 show two patches of echoes, at ∼2345 UT and 0025 UT. Beam 4 shows an additional lower-altitude patch at about 82 km. The echoes start and end at different times for the different beams. To aid in visualizing this, we have plotted two vertical white lines in each subplot, the first of which corresponds to the onset of the first patch of PMSE in beam 4, and the second of which

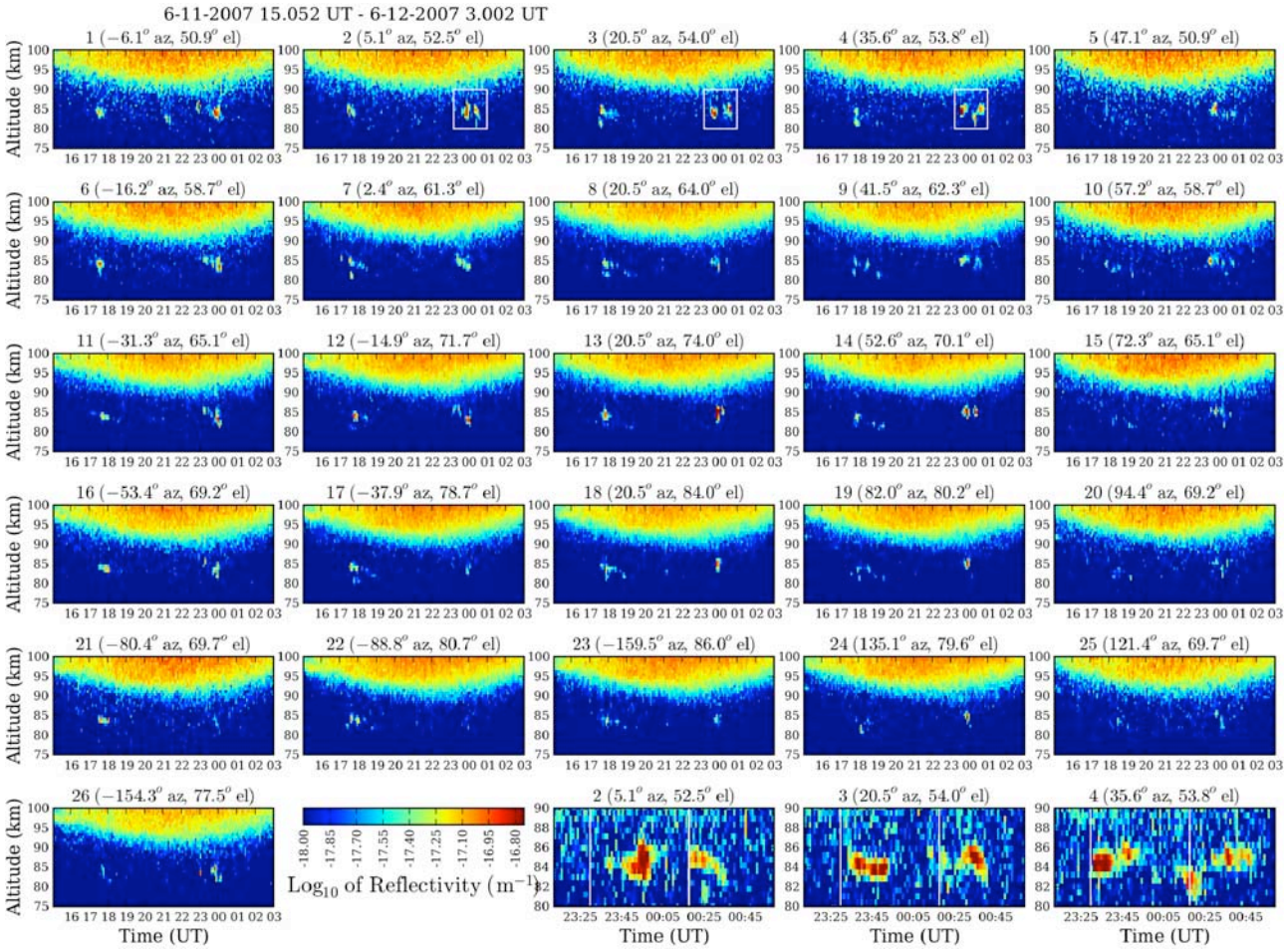

Figure 2. Reflectivity for all 26 beams as a function of time and altitude. Each row of plots corresponds to a row of beams (see Figure 1), arranged from north to south (top to bottom) and west to east (left to right). Beam 26 (lower left) is pointed at the magnetic zenith. The three zoomed-in panels in the lower right show the sections denoted by the white rectangles in beams 2, 3, and 4.

corresponds to the onset of the second patch of PMSE in beam 2. In the first patch, the start time of the echoes moves progressively from beam 4 to beam 2, and for the second patch, the start time moves progressively in the opposite direction. This implies structures that are advecting through the beams.

4. Discussion

4.1. Echo Intensity

[12] The echoes shown in Figure 2 display volume reflectivities in the range expected for PMSE at UHF. *Cho and Kelley* [1993] predicted $\eta \sim 2 \times 10^{-18}$ m^{-1} at 450 MHz for a Schmidt number (ratio of neutral viscosity to plasma diffusion coefficients) of 100. *Rapp and Lübken* [2004, Table 1] summarized the reflectivities reported by different radars as a function of operating frequency. While one must be cautious in comparing signal strengths observed by systems probing in different geophysical regions, the trend of much weaker signals as a function of increasing Bragg scattering wavenumber is very clear. The EISCAT VHF measurements at 224 MHz [e.g., *Hocking and Röttger*, 1997] show reflectivities in the range of $10^{-16} - 10^{-15}$ m^{-1}. The 500 MHz EISCAT Svalbard radar, which is much farther north (near 80°), has observed some weak PMSE, with reflectivities of $\sim 5 \times 10^{-19}$ m^{-1}. This is surprising because the occurrence rates at VHF are very high at these latitudes [*Lübken et al.*, 2004]. Theoretical calculations of the reflectivity do show that it drops very rapidly at these scattering wavelengths, controlled primarily by the Schmidt number and the combination of electron density and irregularity dissipation rate [*Rapp and Lübken*, 2004]. If this is indeed the case, PFISR and ESR may provide an interesting set of frequencies at which to study the phenomenon. The EISCAT UHF system (933 MHz) has observed PMSE with reflectivities close to 10^{-18} m^{-1} [*Röttger et al.*, 1990; *La Hoz et al.*, 2006], which can only be explained by large irregularity dissipation rates and/or very large Schmidt numbers, which implies particles with charge numbers in excess of expectations [*La Hoz et al.*, 2006]. It may well be that a new mechanism is needed to explain the 933 and 1290 MHz observations. The peak reflectivities reported in Figure 2 are in the range of $10^{-17} - 10^{-16}$ m^{-1}. While perhaps somewhat larger than expected, these values are in line with the EISCAT VHF and UHF observations, and the enhanced signal strengths may be tied to the geophysical location of PFISR. These peak values correspond to SNRs of 5–10 dB.

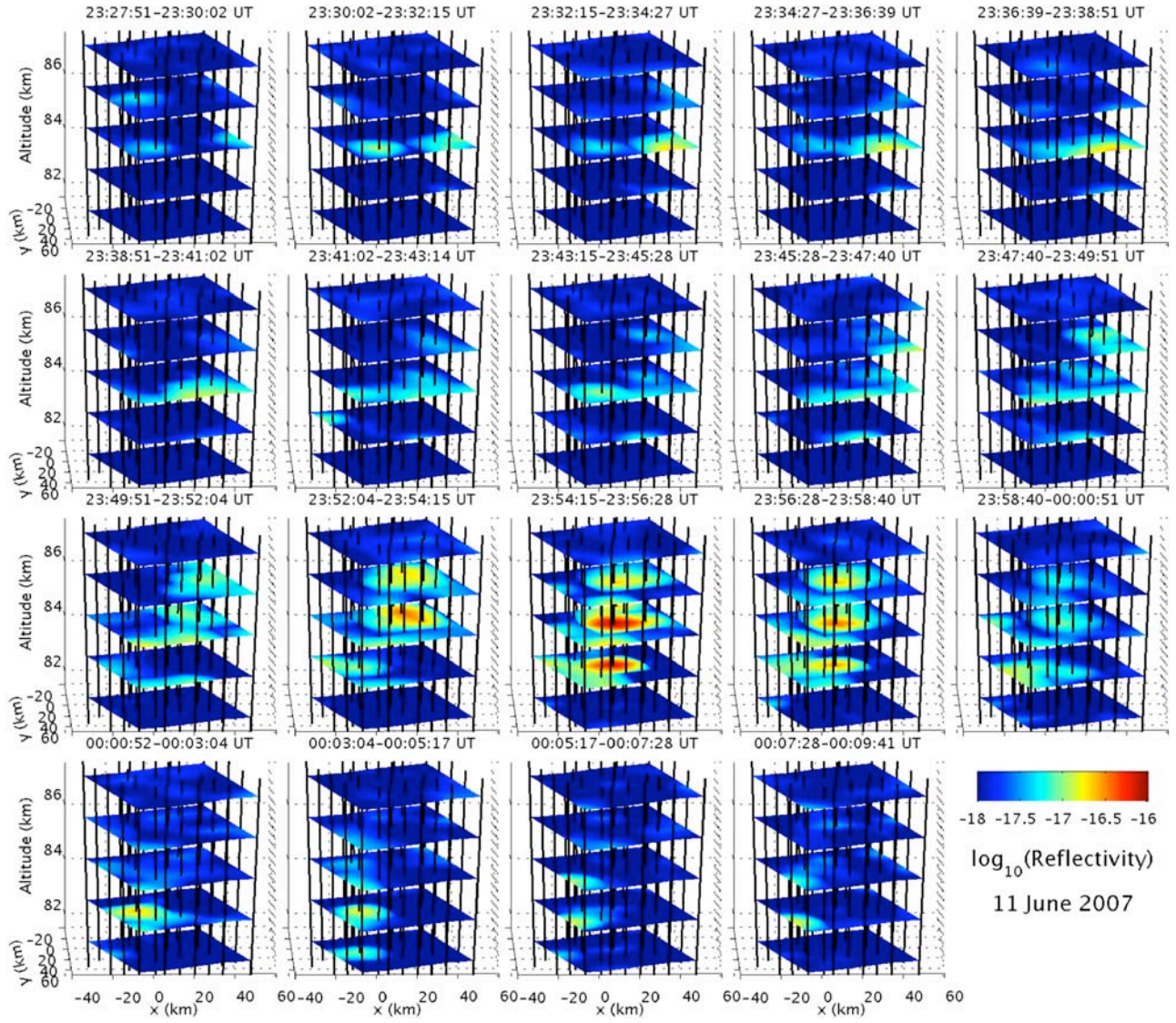

Figure 3. Log_{10} of volume reflectivity from 81.5 to 87.5 km, linearly interpolated and plotted in 3-dimensional format, time series from 2327–0009 UT. The horizontal axes are zonal (x) and meridional (y) distance from the radar location, and the vertical axis is altitude. The vertical lines represent the look direction of the 25 beams used for this grid. Also see the movie in the auxiliary material.

4.2. Aspect Sensitivity

[13] The aspect sensitivity of PMSE is an important parameter relating fundamentally to the scattering mechanism. Some VHF studies [e.g., *Czechowsky et al.*, 1988; *Chilson et al.*, 2002] have shown high aspect sensitivity, meaning that the intensity drops significantly as the radar is scanned away from vertical. Purely isotropic turbulent scatter is expected to display no aspect sensitivity, whereas specular reflections from localized structures within the beam would be expected to be aspect sensitive. It is known from rocket measurements [*Ulwick et al.*, 1988] that PMSE are accompanied by an electron density "biteout" region, associated with electron attachment to the ice particles in the region. *Hocking and Röttger* [1997] argued that specular reflection from the sharp electron density gradient (without associated turbulence) cannot explain observations at VHF, much less at UHF. However, during a rocket experiment, *Alcala and Kelley* [2001] found edges with scales down to 0.3 m and effective η more than 10^{-14} m^{-1} at VHF during a PMSE event. Observations of high aspect sensitivity may also relate to anisotropic turbulence, which seems to be expected (more so at the smaller scales) based on direct numerical simulations [*Werne and Fritts*, 2001; *Achatz*, 2007].

[14] Looking at Figure 2, it does not appear that these echoes are very aspect sensitive, as they are observed in all beams (elevation angles ranging from ~51–86°) with comparable signal levels. We remind the reader that there is no beam pointed exactly vertically, so there could theoretically be aspect-sensitive scatter very close to vertical, but this is not supported by more recent experiments. In order to gauge the aspect sensitivity of the echoes observed by PFISR, we have concentrated on two time periods during which echoes were observed (17–19 and 23–01 UT). In Figure 1, we have plotted the maximum scattered signal within these time periods within the altitude region 82–87 km. We emphasize that the beams are probing different volumes and thus there is

ambiguity in terms of spatial variability of the PMSE and any kind of aspect sensitivity. However, the echoes can be considered homogenous in some sense as they last for tens of minutes and are observed over most of the field-of-view. The maximum value of the echoes shows no strong variation with look direction. In the first time period, the maximum value of the echoes is largest and relatively uniform over the entire western region of the grid. While the peak value during this period is in the beam closest to vertical, this is not repeatable. In the second time period, the strongest echo is at the center of the grid, and there are strong echoes toward the north in the lowest elevation beams. We can only conclude, given the comparatively weak echoes to which PFISR is sensitive and the fact that echoes are observed with relatively constant signal strengths at all probing angles off vertical, that the scatterers do not exhibit a large degree of aspect sensitivity. This implies that the scattering mechanism is likely a volume scattering process associated with isotropic turbulence. Reconciliation with studies that have shown highly aspect sensitive echoes is necessary; it could be that the PMSE that PFISR can observe are not as aspect sensitive, or that there are different scattering mechanisms at work (e.g., enhanced incoherent scatter [*Hagfors*, 1992]). Co-location of a VHF radar with PFISR would be useful for investigating this topic.

4.3. Multi-Beam Visualization

[15] Figures 1 and 2 provide a glimpse of the ability of PFISR to provide new information on the spatial structure and morphology of PMSE. Three-dimensional visualization, however, can be far more enlightening. Figure 3 provides some snapshots from the accompanying movie (see auxiliary material)[1] that displays the three-dimensional observations as a function of time. The axes here are zonal distance (x, positive east), meridional distance (y, positive north), and altitude relative to the radar location. The altitude range is from 81.5–87.5 km in 1.5 km steps (5 slices), and the data from each beam have been linearly interpolated to the appropriate altitude, as well as horizontally between beams. The resolution of this visualization technique is of course limited by the beam spacing. The vertical lines represent the beam look directions and help to line up the different altitude slices. The color again represents the reflectivity on a $\log_{10}$ scale. The movie displays the whole observation period, but in Figure 3 we focus on the ~40 minute time period where the second distinctive patch of echoes are observed, from ~2330–0010 UT.

[16] These snapshots provide evidence for a layer of irregularities drifting into the field-of-view of the system. As discussed earlier, the echoes are seen first in the northeast corner where they appear in the middle altitude bin (84.5 km), grow in strength, and appear to drift westward along the northern edge of the grid, consistent with the interpretation drawn from Figure 2. Multiple patches of echoes appear at different altitudes, and at first seem to be confined to one altitude. However, a strong patch appears at about 2350 UT towards the east, drifts to the center of the grid, and is extended at least 4.5 km in altitude. The echoes intensify and seem to drop in altitude as they disappear. Note that the second blob of irregularities appearing after 0015 UT (discussed earlier) are confined to the northern edge of the grid.

[17] This evidence for drifting structures implies some fossilized irregularity regions of the type proposed by *Rapp and Lübken* [2003] drifting into the field-of-view with the neutral wind. However, there is also significant variability in the echo intensities as they drift around, implying that there are active regions within this scattering layer. Whether these variations are due to regions of active turbulence and/or irregularity development is something to be investigated with co-located instrumentation and spectral measurements.

[18] We also point out, as seen by inspection of Figures 2 and 3, that there are certain times when weak echoes appear in only one or a few beams and last for a short time period, perhaps indicating irregularity development overhead. A possible explanation is that there is a large region of PMSE, that could for example be seen with a VHF system. It is only when the irregularity dissipation rate is enhanced and a cascade to small scales accelerates that the echoes are observed by PFISR. Alternatively, there may be considerable variability in ice particle radii and/or charge number, which determine the Schmidt-number, modulating the UHF scatter. It is also notable that the "sporadic", short-lived echoes seem to occur in general at lower altitudes, which is somewhat surprising since the lifetime of the irregularities is expected to be longer at lower altitudes where the larger ice particles accumulate [e.g., *Rapp and Lübken*, 2004].

5. Conclusion

[19] We have presented observations of PMSE with the PFISR 450 MHz system, which on 11 June 2007 was operating in a mode that allowed for detection in 26 beams separated by ~15–20 km, but did not allow for spectral measurements. The echoes displayed maximum volume reflectivities of around $2–3 \times 10^{-17}$ m^{-1}. There was no evidence for strong aspect sensitive backscatter, as relatively constant intensities were observed at all elevation angles (down to ~50°), implying a volume scattering process associated with isotropic turbulence or enhanced incoherent scatter. Multiple regions of localized (tens of kilometer) echoing regions were observed, appearing to drift in from the north, varying in intensity and altitudinal extent, and lasting for several tens of minutes in any given direction. In addition, some sporadic, shorter-lived irregularities that covered smaller regions were observed, which can be investigated in more detail with the multi-beam capability of PFISR. Coordinated studies with VHF radars, imagers, lidars, and satellites will allow for further investigation of the properties and unresolved issues of PMSE at UHF.

[20] **Acknowledgments.** The PFISR was developed under NSF cooperative agreement ATM-0121483, and the data collection and analysis was supported under NSF cooperative agreement ATM-0608577. The authors thank the University of Alaska Fairbanks, Poker Flat Research Range staff especially Ray Martinez and Brian Lawson for operations and technical support. MJN would like to acknowledge Mary McCready and Roland Tsunoda for comments on a draft of this manuscript.

References

Achatz, U. (2007), Modal and nonmodal perturbations of monochromatic high-frequency gravity waves: Primary nonlinear dynamics, *J. Atmos. Sci.*, *64*, 1977–1994.

[1] Auxiliary materials are available in the HTML. doi:10.1029/2007GL031476.

Alcala, C. M., and M. C. Kelley (2001), Nonturbulent layers in the polar summer mesosphere: 2. Application of wavelet analysis to VHF scattering, *Radio Sci.*, *36*, 891–903.

Balsley, B. B., W. L. Ecklund, and D. C. Fritts (1983), Mesospheric radar echoes at Poker Flat, Alaska: Evidence for seasonally dependent generation mechanisms, *Radio Sci.*, *18*, 1053–1058.

Chilson, P. B., T.-Y. Yu, R. D. Palmer, and S. Kirkwood (2002), Aspect sensitivity measurements of polar mesosphere summer echoes using coherent radar imaging, *Ann. Geophys.*, *20*, 213–223.

Cho, J. Y. N., and M. C. Kelley (1993), Polar mesosphere summer radar echoes, *Rev. Geophys.*, *31*, 243–265.

Cho, J. Y. N., and J. Röttger (1997), An updated review of polar mesosphere summer echoes: Observation, theory, and their relationship to noctilucent clouds and subvisible aerosols, *J. Geophys. Res.*, *102*, 2001–2020.

Cho, J. Y. N., M. C. Kelley, and C. J. Heinselman (1992), Enhancement of Thomson scatter by charged aerosols in the polar mesosphere: Measurements with a 1.29 GHz radar, *Geophys. Res. Lett.*, *19*, 1097–1100.

Czechowsky, P., R. Rüster, and G. Schmidt (1979), Variations of mesospheric structures in different seasons, *Geophys. Res. Lett.*, *6*, 459–462.

Czechowsky, P., I. M. Reid, and R. Rüster (1988), VHF radar measurements of the aspect sensitivity of the summer polar mesopause echoes over Andenes (69°N, 16°E), Norway, *Geophys. Res. Lett.*, *15*, 1259–1262.

Ecklund, W. L., and B. B. Balsley (1981), Long term observations of the arctic mesosphere with the MST radar at Poker Flat, Alaska, *J. Geophys. Res.*, *86*, 7775–7780.

Hagfors, T. (1992), Note on the scattering of electromagnetic waves from charged dust particles in a plasma, *J. Atmos. Terr. Phys.*, *54*, 333–338.

Hall, C. M., and J. Röttger (2001), Initial observations of Polar Mesospheric Summer Echoes using the EISCAT Svalbard Radar, *Geophys. Res. Lett.*, *28*, 131–134.

Hocking, W. K., and J. Röttger (1997), Studies of polar mesosphere summer echoes over EISCAT using calibrated signal strengths and statistical parameters, *Radio Sci.*, *32*, 1425–1444.

Kelley, M. C., and J. C. Ulwick (1988), Large and small-scale organization of electrons in the high-latitude mesosphere: Implications of the STATE data, *J. Geophys. Res.*, *93*, 7001–7008.

Kelley, M. C., D. T. Farley, and J. Röttger (1987), The effect of cluster ions on anomalous VHF backscatter from the summer polar mesosphere, *Geophys. Res. Lett.*, *14*, 1031–1034.

La Hoz, C., O. Havnes, L. I. Næsheim, and D. L. Hysell (2006), Observations and theories of Polar Mesospheric Summer Echoes at a Bragg wavelength of 16 cm, *J. Geophys. Res.*, *111*, D04203, doi:10.1029/2005JD006044.

Lübken, F.-J., G. Lehmacher, T. Blix, U.-P. Hoppe, E. Thrane, J. Cho, and W. Swartz (1993), First in-situ observations of neutral and plasma density fluctuations within a PMSE layer, *Geophys. Res. Lett.*, *20*, 2311–2314.

Lübken, F.-J., M. Rapp, and P. Hoffmann (2002), Neutral air turbulence and temperatures in the vicinity of polar mesosphere summer echoes, *J. Geophys. Res.*, *107*(D15), 4273, doi:10.1029/2001JD000915.

Lübken, F.-J., M. Zecha, J. Höffner, and J. Röttger (2004), Temperatures, polar mesosphere summer echoes, and noctilucent clouds over Spitsbergen (78°N), *J. Geophys. Res.*, *109*, D11203, doi:10.1029/2003JD004247.

Rapp, M., and U.-P. Hoppe (2006), A reconsideration of spectral width measurements in PMSE with EISCAT, *Adv. Space Res.*, *38*, 2408–2412.

Rapp, M., and F.-J. Lübken (2003), On the nature of PMSE: Electron diffusion in the vicinity of charged particles revisited, *J. Geophys. Res.*, *108*(D8), 8437, doi:10.1029/2002JD002857.

Rapp, M., and F.-J. Lübken (2004), Polar mesosphere summer echoes (PMSE): Review of observations and current understanding, *Atmos. Chem. Phys.*, *4*, 2601–2633.

Röttger, J., M. T. Rietveld, C. La Hoz, C. Hall, M. C. Kelley, and W. E. Swartz (1990), Polar mesosphere summer echoes observed with the EISCAT 933-MHz radar and the CUPRI 46.9-MHz radar, their similarity to 224-MHz radar echoes, and their relation to turbulence and electron density profiles, *Radio Sci.*, *25*, 671–687.

Ulwick, J. C., K. D. Baker, M. C. Kelley, B. B. Balsley, and W. L. Ecklund (1988), Comparison of simultaneous MST radar and electron density probe measurements during STATE, *J. Geophys. Res.*, *93*, 6989–7000.

Werne, J., and D. C. Fritts (2001), Anisotropy in a stratified shear layer, *Phys. Chem. Earth Part B*, *26*, 263–268.

C. J. Heinselman, E. A. Hope, J. D. Kelly, M. J. Nicolls, and S. Ranjan, Center for Geospace Studies, SRI International, 333 Ravenswood Avenue, Menlo Park, CA 94025, USA. (michael.nicolls@sri.com)

M. C. Kelley, School of Electrical and Computer Engineering, Cornell University, 320 Rhodes Hall, Ithaca, NY 14853, USA.